DOI: 10.2478/sbeef-2024-0005

STUDY THE EMITTER-BASE FORWARD CURRENT IN HETEROJUNCTION BIPOLAR TRANSISTORS USING PYTHON

G. PREDUȘCĂ, MIRUNA AVRAM
Valahia University of Targoviste, Faculty of Electrical Engineering, Electronics, and Information Technology
E-mail: gabriel.predusca@valahia.ro, adina.avram.ie@valahia.ro

Abstract. ***In GaAs-type materials, the primary mechanism for intra-valley scattering of low-energy electrons is their interaction with acoustic photons. These collisions are of the elastic and isotropic type, with their main effect being the nearly uniform scattering of the velocity vector of the electrons. Since the drift current in heterojunction bipolar transistors is proportional to the electric field, the contribution of the majority drift current cannot be neglected, as even a very small internal field produces a significant current when the number of carriers is very high. At the metallurgical heterojunction (x = 0), the total current is equal to the sum of the two thermionic emission components. The paper analyses the variation of the direct current of the Al0.3Ga0.7As/GaAs heterojunction, used as an emitter-base NP junction in heterojunction bipolar transistors, using the Python program.***

Keywords: heterojunction bipolar transistors, direct current, AlGaAs, Python.

1. INTRODUCTION

In the neutral region (-n), adjacent to the transition zone (w) of a directly polarized PN junction, two different carrier flows are formed: a flow consisting of majority electrons migrating by diffusion from the -n region to the -p region, and a flow consisting of holes in the -p region diffusing into the -n region, becoming excess minority carriers in this region. The holes disappear through recombination with majority electrons at an average distance equal to the diffusion length (L_p), which is much smaller than the thickness (L_n) of the neutral region (-n).

The flow of electrons heading towards the junction, leaving the deep volume zone of the neutral region (-n), must continuously sustain both processes. The source providing the necessary electrons is the metallic contact applied to the semiconductor of type -n.

In the steady state, the total current (J) flowing through the device is a conservative quantity, remaining constant at any point. It comprises both electron and hole components. In the region adjacent to the junction, there is a gradient of majority carriers and a gradient of minority carriers, implicitly resulting in the diffusion current components $J_{n,dif(x)}$ and $J_{p,dif(x)}$. In the deeper regions of the neutral zone, excess minority carriers disappear, along with the diffusion component.

The total current consists solely of majority electrons. In this region, there is no majority concentration gradient, and apparently, there is no electric field either. However, the effective conduction mass of electrons (m_n^{**}) is lower than that of holes (m_p^{**}). Consequently, the mobility of holes (μ_p) is lower than that of electrons (μ_n). This disparity results in a delay in the displacement of a packet of excess holes (Δp) compared to the electron packet (Δn).

The condition of quasi-neutrality, where $\Delta n(x) = \Delta p(x)$, is violated. Due to this violation, a local net charge appears in the volume of the neutral region (-n), given by $\rho V(x) = \Delta n(x) - \Delta p(x) \neq 0$. This, in turn, generates a very small internal electric field, $E_{n,int} \neq 0$.

Since the drift current is proportional to the field ($J_{n,drift} = q\mu_n E$), and the ratio $J_{p,drift}/J_{n,drift}$ is approximately $p/n \approx 10^5/10^{15} = 10^{-10}$, it follows that the contribution of the majority drift current cannot be neglected. Even with a very small internal field, a significant current is produced when the number of carriers is very large. Therefore, in the neutral region (-n), far away from the junction, the current is purely electronic and is determined by the majority drift, resulting from the presence of a very weak internal electric field. This rationale is attributed to Shockley, who provided experimental proof along with Hynes in 1951 [1-4].

2. THERMOELECTRONIC EMISSION CURRENT THROUGH AN AlGaAs/GaAs HETEROJUNCTION

2.1. Directly polarized heterojunctions.

The movement of electrons in the semiconductor is disrupted by collisions with network imperfections, with the most frequent disturbances arising from the vibrations of the crystal, leading to electron-phonon interactions.

In AIII-BV materials, the coupling between an electron and a vibration mode can occur in two ways: polar and non-polar. In the polar case, coupling is achieved through Columbian interaction, while in non-polar coupling, interaction occurs due to local deformation of the crystal potential.

During interaction with a photon, the electron moves in its energy band diagram by either losing or gaining energy quanta. There are two types of transitions: intra-valley transitions, which keep the electron in the energy valley where it was before the collision, and inter-valley transitions, where the electron moves from one energy valley to another.

In GaAs-type materials, the primary mechanism for intra-valley scattering of low-energy electrons is their interaction with acoustic photons. These collisions are of the elastic and isotropic type, with their main effect being

the practically uniform scattering of the velocity vector of the electrons.

For electrons with high energy exceeding the energy of a polar optical photon (35 meV in GaAs), the dominant process of intravalley interaction is the emission of a polar optical photon. This interaction is anisotropic, meaning that as an electron in an electric field gains energy, it deviates less from its trajectory. Despite the energy loss due to the emission of the optical photon, the electron is transported faster in the direction of the electric field that accelerates it. This characteristic explains the high electron mobility observed in AIII-BV semiconductors.

An electron in the energy valley of the emitter's conduction band scales the potential barrier and is emitted into the energy valley of the base. Here, it undergoes a sudden drop, equal to ΔE_C, in its potential energy. Consequently, its kinetic energy increases by an amount of approximately 0.3 eV. The main scattering mechanism on the network becomes the emission of polar optical photons. Since this process is anisotropic, the electron speed distribution at the heterojunction becomes strongly asymmetric. As a result, the transport mechanism shifts from diffusion to a thermoelectric emission mechanism, like that of a Schottky diode.

Ballistic electrons injected into the base will form two distinct populations: quasi-ballistic electrons that have undergone few collisions and are not yet thermalized, and electrons that have undergone more collisions, causing the velocity distribution to become almost isotropic.

Near the heterojunction, the current is determined by the transport of quasi-ballistic electrons, while at a greater distance from the heterojunction, the current is diffusive, attributed to thermalized electrons. In contrast to what occurs in a PN homojunction, carrier injection in a heterojunction involves the thermalization of the ballistic flux in the base.

From a mathematical perspective, the treatment is like that of a homojunction. At the metallurgical heterojunction (x=0), the total current will be the sum of the two components of thermionic emission (Figure 1) [2, 5, 6].

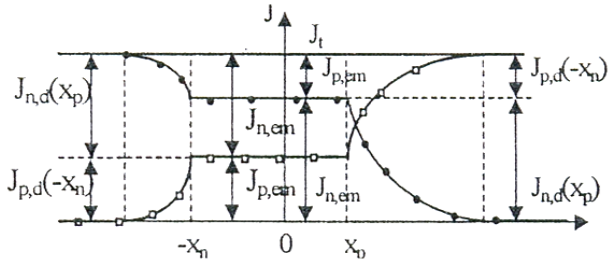


Figure 1. Spatial variation of the current density through a NP homojunction

Through the thermalization of the injected carriers, this current undergoes a transformation into a diffusion current, allowing us to express it as follows:

$$J_t(x) = J_t(0) = J_{n,d}(x_p) + J_{p,d}(-x_n), \qquad (1)$$

where the minority diffusion components are given by the relations:

$$J_{n,d}(x) = qD_n \frac{dn}{dx} \text{ and } J_{p,d}(x) = -qD_n \frac{dp}{dx} \qquad (2)$$

The essential difference compared to the homojunction case is that the minority carrier densities at the edges of the transition region that appear in these expressions can no longer be calculated with the quasi-equilibrium relations:

$$p(-x_n) = \frac{n_i^2}{N_D} exp\left(\frac{qV_a}{kT}\right) \text{ and } n(x_p) = \frac{n_i^2}{N_A} exp\left(\frac{qV_a}{kT}\right) \qquad (3)$$

In this case, they lose their validity and the quantities $p(-x_n)$, $n(x_p)$ is deduced from the continuity conditions:

$$J_{p,d}(-x_n) = J_{p,em} \text{ , } J_{n,d}(x_p) = J_{n,em} \qquad (4)$$

In the immediate vicinity of the x_j heterojunction, taken as the origin of the 0x axis in the figure below, the electrons in the emitter have a higher energy than the electrons in the base, $E_n(x_j) > E_n(x^+_j)$ (Figure 2).

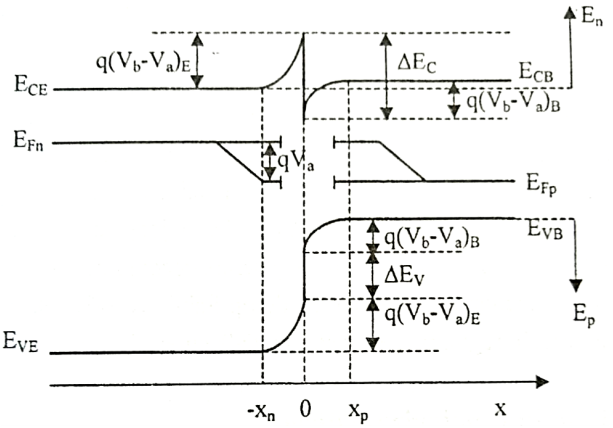


Figure 2. Band diagram of the forward-biased emitter-base heterojunction.

2.2. Calculation of the direct current of the AlGaAs/GaAs heterojunction

The electrons passing from the emitter to the base do not meet a potential barrier and the electron current density injected from the left to the right of the heterojunction is [2]:

$$J_n(x_j, \rightarrow) = q\overline{v}_{x+} n(x_j^-) \qquad (5)$$

Where $\overline{v}_{x+}$ is the average value of the part v_x of the speed v of the electrons climbing the barrier from left to right, $v_x \geq 0$.

When passing from the base to the emitter, the electrons meet a potential barrier:

$$E_n(x_j^-) - E_n(x_j^+) = \Delta E_c \qquad (6)$$

For this reason, the electron current injected from the base to the emitter is:

$$J_n(x_j,\leftarrow) = -q\overline{v}_{x^+} n(x_j^+)\, exp\left(-\frac{\Delta E_c}{kT}\right) \quad (7)$$

The expression of the electron current injected by thermoelectric emission into the metallurgical emitter-base heterojunction is:

$$J_{n,em} = q\overline{v}_{x^+}\left[n(x_j^-) - n(x_j^+)\, exp\left(-\frac{\Delta E_c}{kT}\right)\right] \quad (8)$$

The concentrations $n(x^+_j)$ and $n(x^-_j)$ depending on the electron concentration at the edge of the transition region, if the Fermi quasi-levels are constant up to the vicinity of the metallurgical heterojunction, can be expressed as follows:

$$n(x_j^+) = n(x_p)\, exp\left[\frac{q(V_{bB}-V_{aB})}{kT}\right] \quad (9)$$

$$n(x_j^-) = n(-x_n)\, exp\left[-\frac{q(V_{bE}-V_{aE})}{kT}\right] \quad (10)$$

The concentration $n(-x_n)$ is the concentration of majorities and, according to the general hypothesis: $n(-x_n) = N_D + \hat{n} \approx N_D$, it is equal to N_D. The size $n(x_p)$ is the concentration of minorities from the base at $x=x_p$. The calculation relation $n(x_p) = \frac{n_i^2}{N_A} exp\left(\frac{qV_a}{kT}\right)$, is valid only in the case of homojunction, not in the case of heterojunction. In the case of the heterojunction, the concentration $n(x_p)$ can only be found using the condition: $J_{n,d}(x_p)=J_{n,em}$. Being a continuous quantity, the thermoelectric emission current from the metallurgical heterojunction must be equal to the minority diffusion current from the neutral base, next to the transition region.

Another, more direct, method of calculating the thermoelectric injection current is:

$$nJ_{n,em} = q\overline{v}_{x^+} N_D\, exp\left(-\frac{qV_{bE}}{kT}\right) exp\left(\frac{qV_{aE}}{kT}\right) + C \quad (11)$$

Considering that the potential barrier for holes is much higher than that for electrons, we can ignore the contribution of holes that manage to climb the barrier. Thus, the constant C is found from the equilibrium condition: $J_t \approx J_{n,em}=0$, for $V_a=0$, it results:

$$J_{n,em} = q\overline{v}_{x^+} N_D\, exp\left(-\frac{qV_{bE}}{kT}\right)\left[exp\left(\frac{qV_{aE}}{kT}\right) - 1\right] \quad (12)$$

The average speed $\overline{v}_{x^+}$ is given by the relation:

$$\overline{v}_{x^+} = \left(\frac{kT}{2\pi m_n^*}\right)^{\frac{1}{2}} \quad (13)$$

Using this result, the expression for the injection current can be put in the form of a Richardson type law:

$$J_n = q\overline{v}_{x^+} N_c\, exp\left(-\frac{E_{CE}-E_{Fn}+qV_{bE}}{kT}\right)\left[exp\left(\frac{qV_{aE}}{kT}\right) - 1\right] \quad (14)$$

But,

$$q\overline{v}_{x^+} N_c = \frac{4\pi q m_n^* k^2}{h^3} T^2 \quad (15)$$

Or

$$q\overline{v}_{x^+} N_c = A^* T^2 \quad (16)$$

Were,

$$A^* = \frac{4\pi q m_n^* k^2}{h^3} \quad (17)$$

is Richardson's constant.

Thus, the electron current injected by thermoelectric emission into the emitter-base metallurgical heterojunction is:

$$J_{n,em} = A^* T^2\, exp\left(-\frac{q\phi_0}{kT}\right)\left[exp\left(\frac{qV_{aE}}{kT}\right) - 1\right] \quad (18)$$

Were,

$$q\phi_0 = qV_{bE} + (E_{CE} - E_{Fn}) \quad (19)$$

The voltage drops on the transition regions of the heterojunction are given by the relations:

$$V_{bE} = k_E V_b, V_{bB} = k_B V_b, V_{aE} = k_E V_a, V_{aB} = k_B V_a \quad (20)$$

Were,

$$k_E = \frac{\varepsilon_B N_A}{\varepsilon_E N_D + \varepsilon_B N_A} \text{ and } k_B = \frac{\varepsilon_E N_D}{\varepsilon_E N_D + \varepsilon_B N_A} \quad (21)$$

Noting with: $m = \frac{1}{k_E} = 1 + \frac{\varepsilon_E N_D}{\varepsilon_B N_A}$ becomes:

$$J_{n,em} = A^* T^2\, exp\left(-\frac{q\phi_0}{kT}\right)\left[exp\left(\frac{qV_{aE}}{mkT}\right) - 1\right] \quad (22)$$

where m is the ideality coefficient of the electron current injected by the directly polarized emitter-base heterojunction.

3. ANALYSIS OF THE NP HETEROJUNCTION TYPE AlGaAs/GaAs IN THE CONDITION $N_A >> N_D$

For $N_A >> N_D$ we have m=1; $k_E=1$; $V_{be}=V_b=V_0$ [2, 9].

$$exp\left(-\frac{q\phi_0}{kT}\right) = exp\left[-\frac{qV_0}{kT} + ln\left(\frac{N_D}{N_{CE}}\right)\right] = \frac{N_D}{N_{CE}} exp\left(-\frac{qV_0}{kT}\right) \quad (23)$$

But,

$$\frac{qV_0}{kT} = \frac{\Delta E_C + E_{gB}}{kT} + ln\left(\frac{N_A N_D}{N_{CE} N_{VB}}\right) \quad (24)$$

Result:

$$exp\left(-\frac{q\phi_0}{kT}\right)=\frac{N_D}{N_{CE}}exp\left[-\frac{\Delta E_C+E_{gB}}{kT}-ln\left(\frac{N_AN_D}{N_{CE}N_{VB}}\right)\right]=\frac{N_D}{N_{CE}}\frac{N_{CE}N_{VB}}{N_AN_D}exp\left[-\frac{\Delta E_C+E_{gB}}{kT}\right]=\frac{N_{VB}}{N_A}exp\left[-\frac{\Delta E_C+E_{gB}}{kT}\right] \quad (25)$$

Thus, the electron current injected by thermoelectric emission into the emitter-base metallurgical heterojunction is:

$$J_{n,em}=A^*T^2\frac{N_{VB}}{N_A}exp\left[-\frac{(\Delta E_C+E_{gB})}{kT}\right]\left[exp\left(\frac{qV}{kT}\right)-1\right] \quad (26)$$

But E_{gB}=1,424eV, E_{gE}=1,804eV, ΔE_C=0,322eV, ΔE_V=0,057eV. Results:

$$\Delta E_C+E_{gB}=0{,}322eV+1{,}424eV=1{,}746eV \quad (27)$$

$$\frac{\Delta E_C+E_{gB}}{kT}=\frac{1.746}{25.9*10^{-3}}=\frac{1746}{25.9}=67.48 \quad (28)$$

$$exp\left(-\frac{\Delta E_C+E_{gB}}{kT}\right)=exp(-67.48)=\frac{1}{exp(67.48)}=4.95*10^{-30} \quad (29)$$

$$A^*_{\square}=A^*_n=11.04A/cm^2K^2 \quad (30)$$

$$T=300K \quad (31)$$

Results,

$$A^*T^2=11.04*9*10^4=9.93*10^5A/cm^2 \quad (32)$$

$$N_{VB}=8.3\cdot10^{18}\,cm^{-3} \quad (33)$$

For $N_A=10^{19}$ cm $^{-3}$, we have:

$$\frac{N_{VB}}{N_A}=\frac{8.3*10^{18}}{10^{19}}=0.83 \quad (34)$$

$$A^*\cdot T^2\cdot\frac{N_{VB}}{N_A}\cdot exp\left[-\frac{(\Delta E_C+E_{gB})}{kT}\right]=9.93\cdot10^5\cdot0.83\cdot4.95*10^{-30}=4.04*10^{-24}A/cm^2 \quad (35)$$

Results:

$$J_{n.em}=4.04*10^{-24}*\left[exp\left(\frac{V}{25.9*10^{-3}}\right)-1\right] \quad (36)$$

$$J_{n.em}=4.04*10^{-24}*\left[exp\left(\frac{1000V}{25.9}\right)-1\right] \quad (37)$$

$$J_{n.em}=K*\left[exp\left(\frac{1000V}{25.9}\right)-1\right] \quad (38)$$

4. DIRECT CURRENT VARIATION OF $Al_{0.3}Ga_{0.7}As/GaAs$ HETEROJUNCTION USED AS EMITTER-BASE NP JUNCTION IN HBT TRANSISTORS USING PYTHON

Python is a versatile and widely-used programming language known for its simplicity and readability. It has gained popularity in various fields, including scientific research and data analysis, due to its extensive libraries and ease of use.

Python provides a powerful platform for studying and analysing transistor characteristics. Its extensive libraries, such as NumPy and Matplotlib, enable researchers and engineers to model, simulate, and visualize the behaviour of transistors, facilitating a deeper understanding of their performance. Python has become a go-to language for researchers and engineers in the field of electronics. Its simplicity, coupled with powerful numerical and scientific computing capabilities, makes it a preferred choice for analysing complex semiconductor device characteristics, including those of bipolar transistors [7-9].

Based on the studies, we simulated the variation of the direct current of the $Al_{0.3}Ga_{0.7}As/GaAs$ heterojunction [10-12] used as an emitter-base NP junction in HBT transistors using the Python program in two cases: the results from [2] (Figures 3-5 and Table 1) and the results from [13-14] (Figures 6-8 and Table 2)

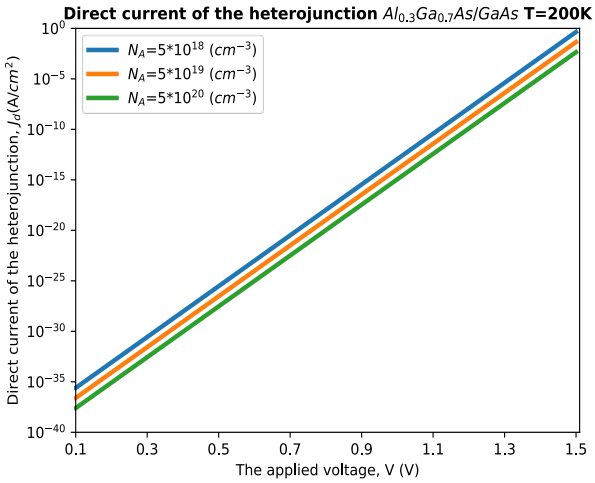


Figure 3. The variation of the direct current of the $Al_{0.3}Ga_{0.7}As/GaAs$ heterojunction depending on the applied voltage, for T=200K, according to the data from [2]

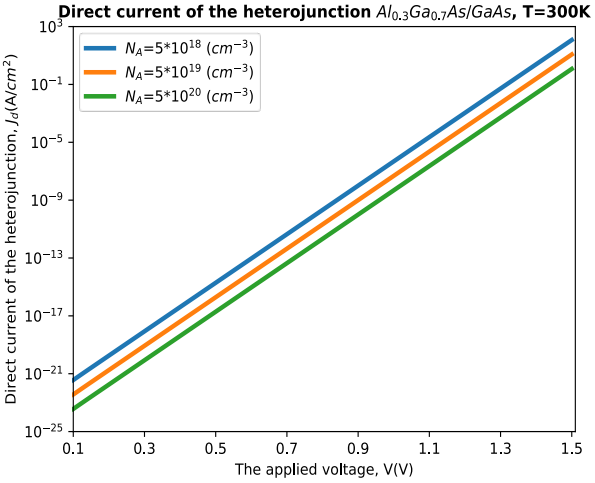


Figure 4. The variation of the direct current of the $Al_{0.3}Ga_{0.7}As/GaAs$ heterojunction depending on the applied voltage, for T=300K, according to the data from [2]

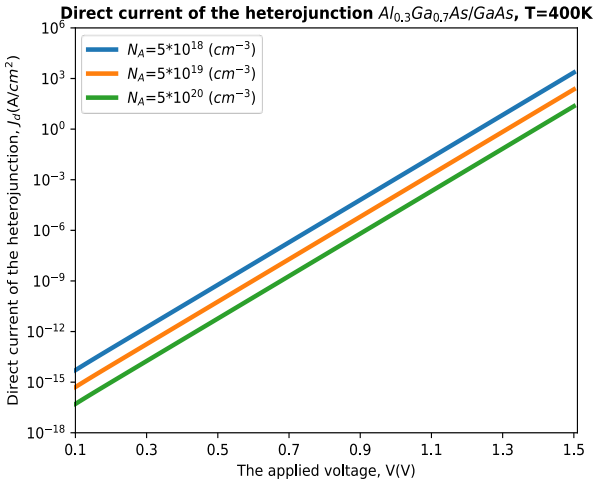


Figure 5. The variation of the direct current of the $Al_{0.3}Ga_{0.7}As/GaAs$ heterojunction depending on the applied voltage, for T=400K, according to the data from [2]

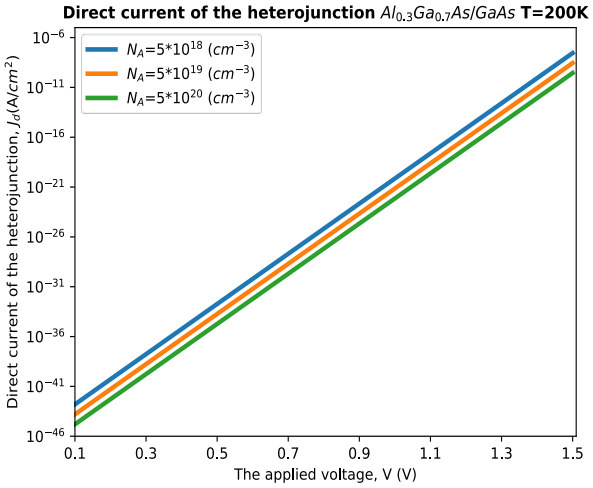


Figure 6. The variation of the direct current of the $Al_{0.3}Ga_{0.7}As/GaAs$ heterojunction depending on the applied voltage, for T=200K, according to the data from [13-14]

Table 1. Results obtained according to the data in [2]

T [K]	K	N_A [cm^{-3}]	J_{direct} (A/cm^2)	
			min	max
200	$7.61 \cdot 10^{-39}$	$5 \cdot 10^{18}$	$5.685 \cdot 10^{-36}$	0.443
	$7.61 \cdot 10^{-40}$	$5 \cdot 10^{19}$	$5.685 \cdot 10^{-37}$	0.0443
	$7.61 \cdot 10^{-41}$	$5 \cdot 10^{20}$	$5.685 \cdot 10^{-38}$	0.00443
300	$7.85 \cdot 10^{-24}$	$5 \cdot 10^{18}$	$6.389 \cdot 10^{-22}$	117.88
	$7.85 \cdot 10^{-25}$	$5 \cdot 10^{19}$	$6.389 \cdot 10^{-23}$	11.788
	$7.85 \cdot 10^{-36}$	$5 \cdot 10^{20}$	$6.389 \cdot 10^{-24}$	1.1788
400	$2.98 \cdot 10^{-20}$	$5 \cdot 10^{18}$	$7.871 \cdot 10^{-15}$	2279.12
	$2.98 \cdot 10^{-21}$	$5 \cdot 10^{19}$	$7.871 \cdot 10^{-16}$	227.912
	$2.98 \cdot 10^{-22}$	$5 \cdot 10^{20}$	$7.871 \cdot 10^{-17}$	22.7912

Upon examining Figures 3-5 and Table 1, a noteworthy trend emerges: the Richardson constant experiences a substantial decrease of 10^3 and 10^{16} times, respectively, in comparison to the baseline case at T=200K, as the temperature varies. This notable shift, combined with a simultaneous reduction in N_A doping concentration, precipitates a considerable surge in the direct current. Specifically, the direct current, initially measured at 0.443 A/cm^2 for T=200K, escalates to 117.88 A/cm^2 at T=300K and further soars to 2279.1 A/cm^2 at T=400K. These observations are made under an applied voltage of V=1.5V.

This trend underscores the sensitivity of the Richardson constant and the direct current to changes in temperature and doping concentration. The significant increase in direct current is a result of the interplay between these variables, shedding light on the complex dynamics governing the behaviour of the $Al_{0.3}Ga_{0.7}As/GaAs$ heterojunction, particularly when employed as an emitter-base NP junction in HBT transistors.

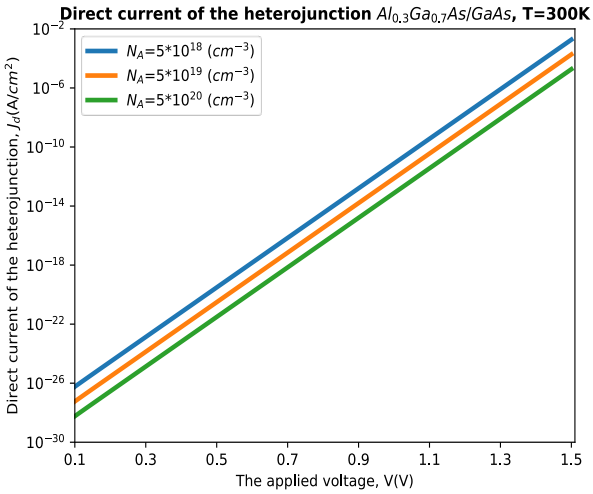


Figure 7. The variation of the direct current of the $Al_{0.3}Ga_{0.7}As/GaAs$ heterojunction depending on the applied voltage, for T=300K, according to the data from [13-14]

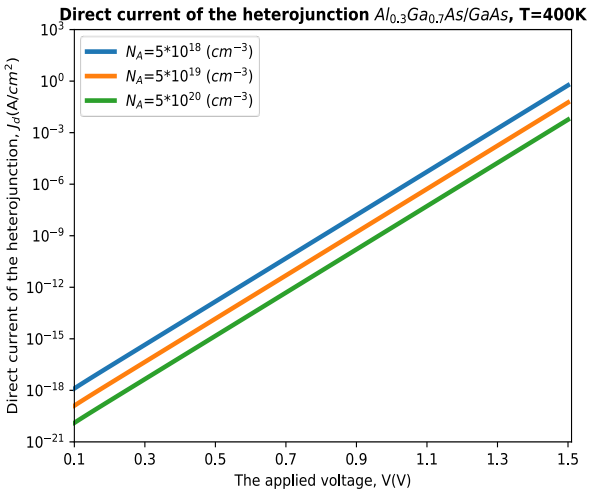


Figure 8. The variation of the direct current of the $Al_{0.3}Ga_{0.7}As/GaAs$ heterojunction depending on the applied voltage, for T=400K, according to the data from [13-14]

Table 2. Results obtained according to the data in [13-14]

T [K]	K	N_A [cm^{-3}]	J_{direct}	
			min	max
200	$4.79 \cdot 10^{-46}$	$5 \cdot 10^{18}$	$3.583 \cdot 10^{-43}$	$2.792 \cdot 10^{-8}$
	$4.79 \cdot 10^{-47}$	$5 \cdot 10^{19}$	$3.583 \cdot 10^{-44}$	$2.792 \cdot 10^{-9}$
	$4.79 \cdot 10^{-48}$	$5 \cdot 10^{20}$	$3.583 \cdot 10^{-45}$	$2.792 \cdot 10^{-10}$
300	$1.24 \cdot 10^{-28}$	$5 \cdot 10^{18}$	$1.011 \cdot 10^{-26}$	0.00186
	$1.24 \cdot 10^{-29}$	$5 \cdot 10^{19}$	$1.011 \cdot 10^{-27}$	0.000186
	$1.24 \cdot 10^{-30}$	$5 \cdot 10^{20}$	$1.011 \cdot 10^{-28}$	$1.86 \cdot 10^{-5}$
400	$7.501 \cdot 10^{-20}$	$5 \cdot 10^{18}$	$1.976 \cdot 10^{-18}$	0.572
	$7.501 \cdot 10^{-21}$	$5 \cdot 10^{19}$	$1.976 \cdot 10^{-19}$	0.0572
	$7.501 \cdot 10^{-22}$	$5 \cdot 10^{20}$	$1.976 \cdot 10^{-20}$	0.00572

Upon scrutinizing the data presented in Figures 6-8 and Table 2, a discernible trend emerges: the Richardson constant experiences a remarkable reduction by factors of 10^3 and 10^{25}, respectively, when compared to the reference case at T=200K, due to variations in temperature. This pronounced alteration, in tandem with a simultaneous decrease in N_A doping concentration, induces a substantial augmentation in the direct current.

To elaborate further, the initial direct current, measured at 2.7921×10^{-8} A/cm^2 for T=200K, undergoes a significant surge to 1.867 mA/cm^2 at T=300K, followed by a decrease to 0.57218 A/cm^2 at T=400K. These variations are recorded under the applied voltage V=1.5V.

The noteworthy changes observed underscore the sensitivity of both the Richardson constant and the resulting direct current to fluctuations in temperature and doping concentration. The observed increase in direct current is a manifestation of the intricate interplay between these influential variables, providing valuable insights into the nuanced dynamics governing the behaviour of the $Al_{0.3}Ga_{0.7}As/GaAs$ heterojunction. This is particularly pertinent when considering its application as an emitter-base NP junction in HBT transistors.

5. CONCLUSIONS

Through a comprehensive analysis, notable changes in the material properties have been identified. The elevation of the forbidden energy band values in the base region, transitioning from E_{gB}=1.425eV to E_{gB}=1.796eV, reflects a considerable modification. Simultaneously, there is an augmentation in the valence band discontinuity, shifting from ΔE_V=0.057eV to ΔE_V=0.138eV, while the conduction band discontinuity experiences a decrease, moving from ΔE_C=0.322eV to ΔE_C=0.237eV.

This orchestrated set of alterations induces a consequential increase in the energy band value within the emitter region, progressing from E_{gE}=1.796eV to E_{gE}=2.171eV. Notably, this elevation in the energy bandgap within the emitter region is linked to a substantial decrease in the forward current.

The intricate relationship between these changes in material parameters underlines the delicate balance required for optimal device performance. The observed increase in the energy bandgap within the emitter region plays a crucial role in dictating the behaviour of the device, notably influencing the forward current. Such insights are pivotal for the design and optimization of semiconductor devices, particularly those involving heterojunctions.

The strategic compositional gradation within the transition region of a heterojunction serves a crucial purpose, particularly in experimental scenarios where adjustments are necessary. This gradation proves instrumental in mitigating the discontinuity observed in both the conduction and valence bands.

The first aspect of this mitigation involves addressing the abrupt increase in the energy of the conduction band. This increase is a direct consequence of the variance in electron bonding energies between the two semiconductor materials forming the heterojunction. By incorporating a compositional gradation in this transition region, engineers and researchers can effectively ameliorate this abrupt jump in conduction band energy.

Simultaneously, the second aspect involves tackling the valence band discontinuity. Here, the compositional gradation of one of the materials within the heterojunction is key. This intentional adjustment in composition helps harmonize the energy levels and facilitates a smoother transition between the semiconductor materials.

In essence, the tailored compositional gradation within the transition region acts as a strategic tool to optimize the performance of the heterojunction. By fine-tuning the material composition, researchers can achieve a more seamless integration of different semiconductor materials, addressing challenges associated with energy band discontinuities and enhancing the overall functionality of the heterojunction in diverse experimental setups.

Heterojunction bipolar transistors find applications in high-frequency devices, amplifiers, and communication systems. Studying the emitter-base forward current in HBTs using Python allows for efficient design and optimization of these devices for specific applications.

6. REFERENCES

[1] D. Sachelarie, Bazele dispozitivelor semiconductoare, MatrixRom, 2003.
[2] D. Sachelarie, Semiconductoare și heterostructuri, MatrixRom, București, 2000.
[3] J.R. Haynes, W. Shockley, The mobility and life of injected holes and electrons in Germanium, Phys. Rev. 81, 835, 1951.
[4] N.A. Al-Ahmadi, H.A. Al-Jawhari, Effect of epitaxial layer thickness on the electrical properties of Ti/n-AlGaAs grown by MBE, Results in Physics 6, 2016, pp.67-69.
[5] A.M. Hashim, F. Mustafa, S.F. Abd Rahman, A.R.A. Rahman, Dual-function on-chip AlGaAs/GaAs Schottky diode for RF power detection and low-power rectenna applications, Sensors, volume 11, issue 8, 2011, pp. 8127-8142.

[6] J.J. Liou, C.H. Huang, AlGaAs/GaAs heterojunctions bipolar transistors for power applications: issues of thermal effects and reliability, Microelectronics Journal, volume 32, 2001, pp.419-431.
[7] V. I. Shivkumar, Simulating nonlinear circuits with Python power electronics, Springer, 2018.
[8] L.A. Ribeiro, Python-based simulation and analysis of electrical circuits through transfer functions, 3rd International Conference on Electrical, Computer, Communications and Mechatronics Engineering (ICECCME), 2023, pp.1-6.
[9] H. Zhang, P. Yang, Y. Niu, Application of Python scientific computing library and simulation in circuit analysis, IEEE 12th International Conference on Communication Systems and Network Technologies (CSNT), 2023, pp.892-898.
[10] J. Batey, S.L. Wright, D.J. DiMaria, Energy band-gap discontinuities in GaAs:(Al,Ga) As heterojunctions, Journal of Applied Physics, Volume 57, Issue 2, January 15, 1985, pp.484-487.
[11] R. Klofkorn, E. Keilegavlen, F. Radu, J. Fuhrmann, Finite volumes for complex applications IX – methods, theoretical aspects, examples, Springer, 2020.
[12] G. Predusca, D. Sachelarie, Matlab pentru microelectronica, Ed. MatrixRom, Bucureşti, 2011.
[13] https://www.ioffe.ru/SVA/NSM/Semicond/AlGaAs/bandstr.html.
[14] https://www.batop.de/information/Eg_AlGaAs.html#.